Journal of Sound and Vibration (1998) **211**(4), 637–661

A REARRANGEMENT OF THE MODAL EXPANSION FOR A DAMPED TWO-DIMENSIONAL VIBRATORY SYSTEM

J. M. MUGGLETON

Department of Mechanical Engineering, Southampton University, Highfield, Southampton SO17 1BJ, England

AND

R. J. PINNINGTON

Institute of Sound and Vibration Research, Southampton University, Highfield, Southampton SO17 1BJ, England

(*Received* 20 *May* 1997, *and in final form* 14 *November* 1997)

When investigating the acoustic or vibrational behaviour of a two- or three-dimensional system, the classical approach is to compute the response as a sum over all contributing modes. In this paper the modal summation of a two-dimensional system is rearranged, taking into account the physical nature of the modes. The modes are grouped according to the direction in which their constituent waves propagate, and are shown to be represented as an array of image line sources. Closed form expressions for the input impedance and the system's transfer impedances are obtained for each mode group. The modal summation is then performed over all contributing mode groups. A line source model is thus generated which approximates to the exact point source model. The closed form solutions obtained enable damping in the medium and at the boundaries to be taken into consideration. For heavy damping, the line source or modal models are shown to be in error. An alternative formulation, which allows for the time delay for line sources to be set up, is presented, with some justification. Results are presented of an experimental validation of the unmodified theory, as it relates to a rigid-walled two-dimensional enclosure. Measurements of input and transfer impedances were made in an air-filled, perspex enclosure. The effect of damping, evenly distributed throughout the enclosure, was investigated. In general, the measured input and transfer impedances show good agreement with the theoretical predictions.

1. INTRODUCTION

The acoustic or vibrational behaviour of two- and three-dimensional systems is of considerable interest in many branches of engineering and physics. In recent years, particularly in the automotive and aerospace industries, much attention has been paid to reducing sound levels in three-dimensional enclosures or to reducing the vibration transmission in plates. Although a considerable amount can often be done to reduce sound and vibration at source, an understanding of the manner of wave propagation enables appropriate design decisions to be made at an early stage. Most acoustic spaces are of non-uniform geometry, and many have large absorption on the surfaces or within the volume, making accurate analysis impossible by any means. There are possibilities of using approximate methods, in which either extremely light or heavy damping is assumed, but these necessarily require many assumptions and provide answers which sometimes lack

0022–460X/98/140637 + 25 $25.00/0/sv971395

detail. The intention here, therefore, is to provide some physical understanding of the relationships between modal and free field behaviour inside a rectangular two-dimensional system by using a model which can include absorption in the medium and at the boundaries, and ultimately provide causal time response information. This will thereby assist possible modification of existing modelling methods. The example chosen here is an acoustic system; however, results are in terms of wavenumber to permit application to all wave types whether non-dispersive or dispersive.

There are a variety of approaches which can be used for the acoustic modelling of a fluid-filled cavity. One alternative is to use the finite element technique [1]. This is generally useful only at low frequencies, and although work has been carried out on regular and irregular shaped cavities to determine the natural frequencies and mode shapes [2–5], even for a rectangular cavity, to the authors' knowledge, no attempt has ever been made to model the damping of each mode. The three most common approaches used in room acoustics, traditional reverberation time methods [6–8], ray tracing [9–13], and image sources [14, 15] are all generally high frequency techniques. The acoustic field usually is assumed to be diffuse: i.e., wave interference is neglected by assuming that their mean intensities are additive. Another approximate approach to this type of problem is Statistical Energy Analysis (S.E.A.) [16], but again, this leads to the requirement, as with the room acoustics approaches, that the acoustic field is effectively diffuse.

The relationship between modal behaviour and boundary absorption has been investigated previously for one-dimensional systems [17, 18] and closed form solutions were provided in which the attenuation and phase change around a return path are the controlling parameters. This analysis is extended here for a corner-excited, two-dimensional, rectangular cavity in which the wave field is decomposed into a set of one-dimensional systems, each with a certain associated path length and attenuation. These two-dimensional parameters are found by first representing the two-dimensional wave field as an array of point image sources. Line arrays of point sources are then approximated as continuous line sources, the direction of which describes one of the equivalent one-dimensional systems. The input and transfer impedances of the line source model correspond to that of the usual modal model [19] for very light damping, indicating that the modal model assumes line sources.

The line source model initially presented is successful for light and even for moderate damping, and can accommodate angle dependent reflection coefficients (if the walls are locally reacting), and with different values on each wall. However, the model is limited to systems described by uncoupled, orthogonal modes, and where the image source model may be applied. Furthermore, if the damping becomes very heavy, the line source assumption is shown to break down, and both the modal model and one-dimensional model as presented become invalid. A modified theory is presented to deal with the heavy damping case, based on the argument that a mode is not set up until wavefronts from an array of point sources have travelled far enough for the combined wavefront to become plane.

Similar results have been derived for three-dimensional acoustic spaces [20]. The main extensions here to this work are the following: the modal summation equivalence to a one-dimensional system; the summation of one-dimensional systems; and a more rigorous treatment of boundary absorption.

Finally, some experimental work is presented, designed to test the unmodified theory, namely a moderately damped two-dimensional enclosure. The transfer functions between pressure and source velocity that were measured were, in general, in good agreement with those predicted from the one-dimensional system sum.

2. MODES IN A TWO-DIMENSIONAL RECTANGULAR CAVITY

The wavenumber vector grid for a hard walled rectangular cavity is described. This is used to identify the directions and modal densities of the equivalent one-dimensional systems. Wavenumbers, rather than frequencies, are used predominantly here as the outcome of the analyses can then be used for plates with either dispersive or non-dispersive waves.

2.1. MODAL FREQUENCIES AND MODAL WAVENUMBERS

Consider a rigid walled rectangular cavity with sides of length l_x and l_y. A potential function $\psi(x, y)$ of the form [19]

$$\psi(x, y) = \cos k_x x \cos k_y y \tag{2.1}$$

satisfies the boundary conditions. Resonance frequencies, ω_N, have associated wavenumbers k_N,

$$k_N^2 = k_x^2 + k_y^2, \tag{2.2}$$

where $k_x = n\pi/l_x$ and $k_y = m\pi/l_y$. The potential function (2.1) can be re-expressed as the sum of four travelling waves with direction vectors $\pm(k_x \mathbf{x} \pm k_y \mathbf{y})$ where $\mathbf{x}$ and $\mathbf{y}$ are unit vectors in the x and y directions respectively:

$$\psi(x, y) = \tfrac{1}{4}[e^{i(k_x x + k_y y)} + e^{-i(k_x x + k_y y)} + e^{i(k_x x - k_y y)} + e^{-i(k_x x - k_y y)}]. \tag{2.3}$$

Each mode can be thought of as a point on a two-dimensional wavenumber vector grid [19, 21], as shown in Figure 1. The x and y component wavenumbers for a mode are the projected distances of the grid point along the x- and y-axes respectively. The resultant wavenumber is the length of the wave vector and the direction of the principal travelling wave (that in the first quadrant) is the direction of the wave vector. The direction of the travelling waves, ϕ_p, is defined by the ratio of the two component wavenumbers:

$$\tan \phi_p = \pm m l_x / n l_y. \tag{2.4}$$

2.2. GROUPING OF MODES

It is possible to assemble the modes on the two-dimensional grid into groups, each with vectors of the same direction. This is shown in Figure 2. All the modes in one group lie on a straight line starting at the origin and are evenly spaced along that line. Any one mode

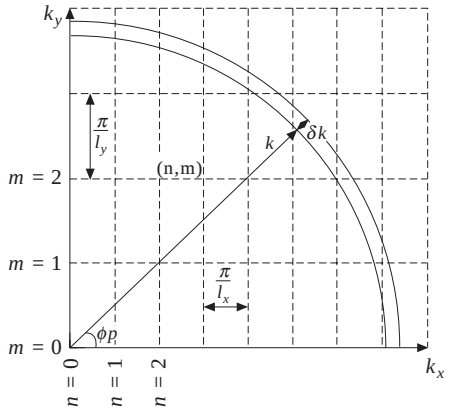

Figure 1. Two-dimensional wavenumber vector grid.

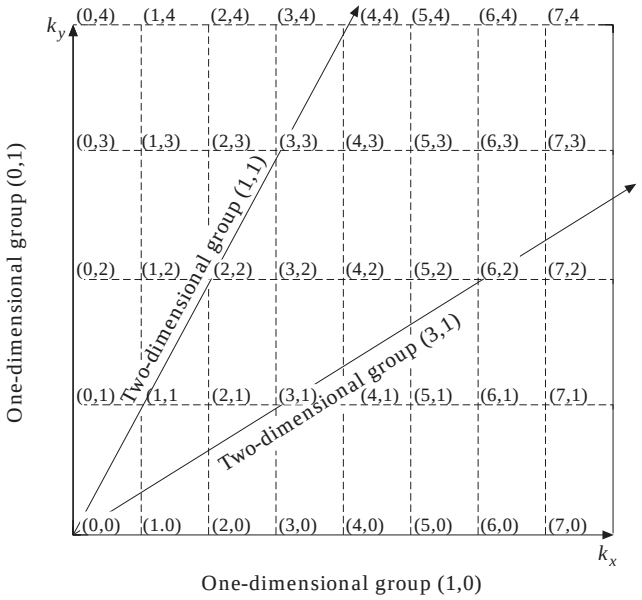

Figure 2. Mode groups on the wavenumber vector grid.

(apart from the (0, 0) mode at the origin) can belong to one mode group only. There are two distinct types of mode group. The (1, 0) and the (0, 1) group which lie along the axes in the wave vector grid are one-dimensional mode groups. The modes in these groups comprise only two travelling waves which propagate parallel to one side of the cavity and produce a one-dimensional mode shape. The modes belonging to the remaining mode groups comprise four travelling wave directions, at an oblique angle to the axes, producing a two-dimensional mode shape. A modal density, which is simply related to the spacing between the modes on a single line, or vector, can be attributed to each mode group of either type. If the angular resonance frequency of the first mode in a group is ω_{M0}, then the associated wavenumber is k_{M0} where

$$k_{M0}^2 = (n\pi/l_x)^2 + (m\pi/l_y)^2. \tag{2.5}$$

The higher resonances of this group are simply integer multiples, q_p, of k_{M0}, giving the modal density in terms of modes per wavenumber as $1/k_{M0}$. The resonance wavenumber at the q_p th mode is therefore

$$k_M = q_p\, k_{M0}. \tag{2.6}$$

The wavelength of the first mode in the group is $\lambda_{M0} = 2\pi/k_{M0}$.

3. TWO-DIMENSIONAL CAVITY REPRESENTED AS A SET OF ONE-DIMENSIONAL SYSTEMS

The corner-excited cavity is represented by an infinite periodic cavity of point image sources which are then regarded as a network of line sources. The equivalent one-dimensional systems are obtained from these line sources. The transfer functions of a single line source are calculated and these are combined to give the total transfer functions of the cavity.

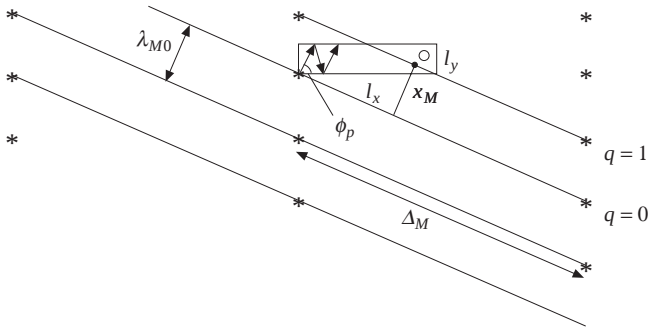

Figure 3. A mode in two dimensions with image sources. ——, Wavefront; →, sound ray; ∗, source; ○, receiver position.

3.1. POINT SOURCE MODEL AND ONE-DIMENSIONAL SYSTEMS

Consider the general fundamental (n, m) mode and all the modes in the same group $(2n, 2m; 3n, 3m;$ etc.) of a rigid walled rectangular cavity with sides l_x and l_y as depicted in Figure 3. A compact volume source is located in one corner of the cavity. The resultant wave field can be thought of as due to the summation of the real source and an infinite number of image sources of equal strength, spaced in a regular grid pattern on the x-y plane [22]. The spacing of the sources in the x and y directions are $2l_x$ and $2l_y$ respectively. Although the volume source excites the fluid in all directions, consider only the four propagation directions associated uniquely with a single mode group.

First, consider the opposing two propagation directions given by ϕ_p and $\phi_p - \pi$. For any given mode group, the sources may be arranged in line perpendicular to these directions. The sources are evenly spaced a distance Δ_M on each line, and the source lines themselves are spaced evenly by the wavelength, λ_{M0} of the first mode in a particular group, $q_p = 1$. Resonances occur in a group when a plane wave from one line source, seen in Figure 4, arrives in phase at the adjacent line source of the same group, or when

$$q_p \lambda = 2l_M, \qquad q_p = 1, 2, 3, \ldots . \tag{3.1}$$

q_p is the mode counter, λ is the wavelength at a particular frequency, and l_M is the length of the equivalent one-dimensional system, which may now be introduced and is described by the line sources.

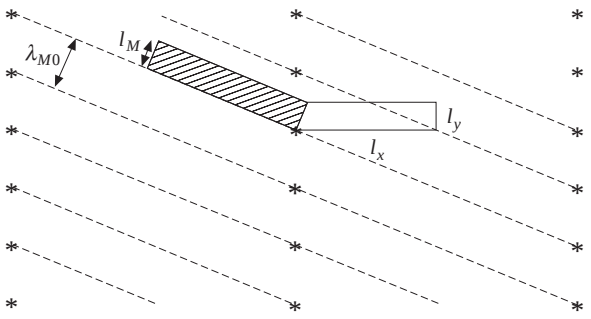

Figure 4. Source representation of a two-dimensional cavity and the line source distribution for the one-dimensional system generated, - - - -, Wavefronts; ∗, 2D system sources; □, 2D cavity; ▨, 1D system.

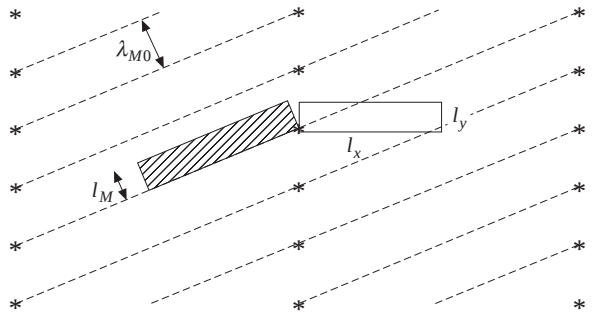

Figure 5. The second one-dimensional system generated. Key as Figure 4.

The periodicity of the image sources causes each equivalent one-dimensional system to have the same area ($A = l_x\, l_y$) as the original two-dimensional cavity, as seen in Figure 4. The source spacing along each line is therefore

$$\Delta_M = 4A/\lambda_{M0}. \tag{3.2}$$

The considerations above allow for two waves in the group. The other two waves would generate a second system identical to the first, but mirrored about the x- or y-axis as shown in Figure 5. The second system has the same properties as the first and does not have to be considered separately.

One-dimensional systems are therefore simply obtained, subject to the requirement that an array of point sources can be thought of as a line source. The limitations of this representation are considered later in section 4.

3.2. TRANSFER FUNCTIONS OF A ONE-DIMENSIONAL SYSTEM

The transfer impedance of an end-excited one-dimensional system is now generated from the sum of a set of image sources, which correspond to line sources in the two-dimensional model.

Figure 6 shows an image source representation of a one-dimensional cavity of length l. A velocity source is placed at $x = 0$ and a reflection coefficient $\bar{r} = r\, e^{i\varepsilon}$ describes the boundary at $x = 1$. The medium has some inherent dissipation mechanism described by a loss factor η, which is accommodated by a complex wavenumber, k. For a non-dispersive medium, $k \approx |k|(1 - i\eta/2)$, while for flexural waves $k \approx |k|(1 - i\eta/4)$, it being assumed that $\eta \ll 1$. The medium has a characteristic impedance ρcS (S being the cross-sectional area), which is mainly real if $\eta \ll 1$, as is assumed here.

The source has a velocity $u_0\, e^{i\omega t}$, causing a right going wave of normalized pressure $p(x)/u_0 = \rho c\, e^{-ikx}$. The $e^{i\omega t}$ dependence is suppressed. The image sources each radiate the same pressure in both directions, modified by the reflection coefficient as indicated in the figure. The normalized force or transfer impedance $Z(x)$ at any point x is the sum of all the source contributions,

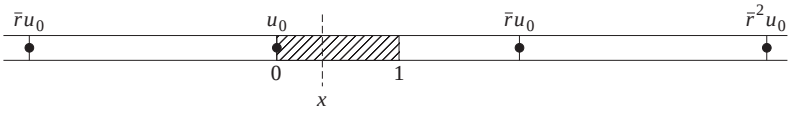

Figure 6. Image source description of a one-dimensional system.

$$Z(x) = \rho cS\,\mathrm{e}^{-\mathrm{i}kx}(1 + \alpha + \alpha^2 + \cdots) + \rho cS\,\mathrm{e}^{\mathrm{i}kx}\alpha(1 + \alpha + \alpha^2 + \cdots), \tag{3.3}$$

where $\alpha = \bar{r}\,\mathrm{e}^{-2\mathrm{i}kl}$ is the total attenuation and phase change in a wave travelling $2l$. A geometric sum gives the transfer impedance to any point x as

$$Z(x) = [(\rho cS/(1 - \alpha)](\mathrm{e}^{-\mathrm{i}kx} + e^{\mathrm{i}kx}\alpha). \tag{3.4}$$

The input impedance at $x = 0$ is

$$Z(0) = \rho cS(1 + \alpha)/(1 - \alpha) \tag{3.5}$$

and the transfer impedance to point $x = l$ is

$$Z(l) = 2\rho cS\,\mathrm{e}^{-\mathrm{i}kl}/(1 - \alpha). \tag{3.6}$$

Equation (3.4) can be rearranged as

$$Z(x) = \rho cS(2\alpha \cos kx/(1 - \alpha) + \mathrm{e}^{-\mathrm{i}kx}), \tag{3.7}$$

showing, for zero damping, the modal and the travelling wave components clearly identified as the first and second terms. The usual modal solutions described by the cos kx term omit the travelling wave term, as it is insignificant for light damping. However, when the damping becomes so large that the attenuation or $|\alpha| \to 0$, only the travelling wave remains. The intention here is to use these wave impedance functions so that they preserve the time delay information under all damping conditions.

If the excitation area, S_0 is not equal to the cross-section, S, continuity of pressure p, and volume velocity, $S_0\,u_0$ are still preserved unchanged. From equation (3.4),

$$p(x)/u_0 = [\rho cS_0\,/S(1 - \alpha)]\,(\mathrm{e}^{-\mathrm{i}kx} + \alpha\,\mathrm{e}^{\mathrm{i}kx}). \tag{3.8}$$

The input impedance $Z(0)$ is obtained by setting the force $F_0 = S_0\,p(0)$ and setting $x = 0$:

$$Z_0 = \rho c[S_0^2\,/S(1 - \alpha)]\,(1 + \alpha). \tag{3.9}$$

If the two-dimensional cavity is depth t, then from Figure 4 and equation (3.2) it can be seen that the cross-sectional area S is given by

$$S = \Delta_M\,t/2 = 2At/\lambda_{M0} = 2V/\lambda_{M0}. \tag{3.10}$$

The excitation area is the same for all source arrangements, so the input impedance $Z_M\,(0)$ from equation (3.9) is

$$Z_M\,(0) = Z_{00}\,(S_0\,\lambda_{M0}\,/2V)/[(1 + \alpha_M)/(1 - \alpha_M)], \tag{3.11}$$

where the wave factor α is altered, $\alpha_M = \bar{r}\,\mathrm{e}^{-\mathrm{i}k\lambda_{M0}}$, and the characteristic impedance $Z_{00} = \rho cS_0$. The reflection coefficient $\bar{r}$ now represents the average value for a wave travelling one circuit of the enclosure, making multiple reflections from each wall. The number of reflections off each surface is a function of the angle of the wave and is described in section 4.2.

The impedance given in equation (3.11) is for a single one-dimensional equivalent system. Each two-dimensional mode group comprises two one-dimensional systems, and therefore the impedance is given by twice equation (3.11). The impedance for a one-dimensional mode group is given directly by equation (3.11).

For illustration, equation (3.11) may be written in complex form for the particular case of a rigid boundary, i.e., $\bar{r} = 1$, by separating the attenuation component from the wave component by setting

$$\alpha_M = |\alpha_M\,|(\cos\theta_M + \mathrm{i}\sin\theta_M),$$

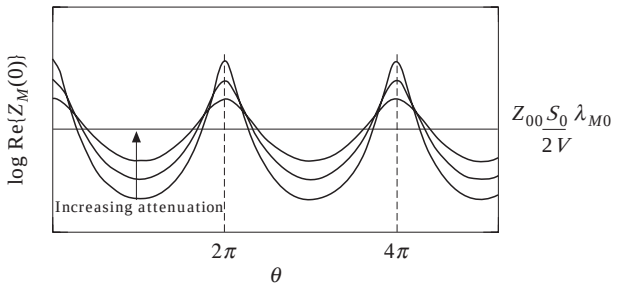

Figure 7. Real part of the impedance of a single mode group.

where $\theta_M = -k\lambda_{M0}$ and $|\alpha_M| = e^{-\eta(k/2)\lambda_{M0}}$ (η is the loss factor; here non-dispersive waves are assumed) giving

$$Z_M(0) = Z_{00}\frac{S_0\,\lambda_{M0}}{2V}\frac{1 - |\alpha_M|^2 + 2i|\alpha_M|\sin\theta_M}{1 + |\alpha_M|^2 - 2|\alpha_M|\cos\theta_M}. \tag{3.12}$$

The real component of this function is plotted in Figure 7 for various values of the attenuation function $|\alpha_M|$.

The resonances occur when $\cos\theta = 1$, causing an increase from the mean by a factor of $(1 + |\alpha_M|)/(1 - |\alpha_M|)$. The troughs occur when $\cos\theta = -1$, dropping below the mean by the same factor. The most interesting feature is that the mean value $\bar{Z}_M(0)$, corresponding to the constant on the left, decreases with decreasing system length, or alternatively, upon using equation (3.10), increasing source distance Δ_M:

$$\bar{Z}_M(0) = \rho c 2S_0^2/\Delta_M t. \tag{3.13}$$

By use of the line source argument the transfer impedance to any point within the enclosure can be found from the perpendicular distance x_M, seen in Figure 3, from the source line through the origin. If the distance from the nearest source line is x:

$$x = x_M - q\lambda_{M0}, \qquad q = 0, 1, 2, \ldots, \tag{3.14}$$

where q counts the number of source lines in the interval x. In Figure 3, $q = 1$. The pressure at position x_M is obtained from equations (3.8) and (3.10) by setting the reflection coefficient to unity, when all the sources are of equal strength. Then, for a single equivalent one-dimensional system

$$p(x_M)/u_0 = (2Z_{00}/\Delta_M t)\,[(e^{-ikx} + \alpha_M e^{ikx})/(1 - \alpha_M)], \tag{3.15}$$

and $\alpha_M = \bar{r}\,e^{-ik\lambda_m}$. For the wave groups $(n, 0)$ and $(0, m)$ the pressure is given directly by equation (3.15). For the two-dimensional mode groups, the pressure is twice this value. The pressure at any point from all the wave sets would be given from a summation over all sets.

This means of calculating the transfer function has been rigorously derived from the modal expansion in section 2. However, a curiosity is revealed in Figure 3, where a source line actually crosses the enclosure, giving a response at the same instance as that of the true point source, without allowing for the travel time from the true source. The implication is that the modal expansion, and this one-dimensional expansion, give acaudal results, and cannot be relied upon in the time domain.

The modal approach or line source description can be applied with confidence only when it is certain that an array of image sources can be regarded as a line source. This is discussed further in section 4.

3.3. COMPARISON WITH CLASSICAL MODAL THEORY

Equivalence of the image source model and the modal solution has long been established for the case of a rigid-walled, lossless, rectangular enclosure [23]. The source line model presented here, which include losses, can now also be compared with the classical modal model. Morse [19] derived an expression for the pressure at any point inside a rectangular cavity due to a volume velocity source. Ignoring the damping term and restricting the result to two dimensions, the pressure at a corner at frequency ω, due to a source at the same corner is given by a simple summation of orthogonal modes,

$$p_0 = \frac{\rho c^2 Q_0}{V} \sum_{n,m} \frac{-\mathrm{i}\varepsilon_n \varepsilon_m \omega}{\omega^2 - \omega_{n,m}^2}, \tag{3.16}$$

where $\omega_{n,m}$ are the modal frequencies, $\varepsilon_0 = 1$, $\varepsilon_1 = \varepsilon_2, \ldots, = 2$, Q_0 is the volume velocity source strength at the corner and V is the cavity volume.

Substituting for Q_0 in terms of a plane velocity source u_0 acting over an area S_0, and expressing the angular frequency, ω, in terms of the wavenumber, k, gives

$$p_0 = \frac{\mathrm{i}\rho c u_0 S_0}{V} \sum_{n,m} \frac{\varepsilon_n \varepsilon_m k}{k_{n,m}^2 - k^2}. \tag{3.17}$$

This sum can be calculated for each mode group separately as no mode other than the (0, 0) mode belongs to more than one group.

For a single mode group, with the (0, 0) mode excluded, the summation can be rewritten by using equation (2.6) as

$$\sum_{n,m} \frac{\varepsilon_n \varepsilon_m k}{k_{n,m}^2 - k^2} = \frac{1}{k_{M0}^2} \sum_{q_p = 1}^{\infty} \frac{\varepsilon_n \varepsilon_m k}{q_p^2 - (k/k_{M0})^2}. \tag{3.18}$$

Performing this summation [24] gives

$$\sum_{q_p = 1}^{\infty} \frac{\varepsilon_n \varepsilon_m k}{k_M^2 - k^2} = \frac{\varepsilon_n \varepsilon_m}{2k_{M0}} \left(-\pi \cot \frac{k\pi}{k_{M0}} + \frac{k_{M0}}{k} \right). \tag{3.19}$$

Returning to equation (3.17), one finds that the total pressure due to each mode group alone, excluding the (0, 0) mode, is then

$$p_0 = \frac{-\mathrm{i}\rho c u_0 S_0}{V} \frac{\varepsilon_n \varepsilon_m}{2} \left(\frac{\lambda_{M0}}{2} \cot \frac{k\lambda_{M0}}{2} - \frac{1}{k} \right). \tag{3.20}$$

When $k\lambda_{M0}/2 \ll 1$, i.e., before the first resonance, the pressure goes to zero as the $M = 0$ term has been excluded. (In fact, the (0, 0) mode dominates the response at zero frequency, with zero wavenumber, and is a volume stiffness for a rigid-walled enclosure, and a rigid mass for a pressure-release boundary.) At higher wavenumbers, the second term can be excluded and the expression becomes

$$Z_M(0) = -\mathrm{i} \frac{Z_{00}}{2V} S_0 \lambda_{M0} \frac{\varepsilon_n \varepsilon_m}{2} \cot \frac{k\lambda_{M0}}{2}. \tag{3.2}$$

For a one-dimensional group, $(n, 0)$ or $(0, m)$, $\varepsilon_n \varepsilon_m = 2$, and equation (3.21) becomes the same as equation (3.11) for light damping. For (n, m) modes, the impedance becomes twice

equation (3.11) as $\varepsilon_n \varepsilon_m = 4$. A one-dimensional system with line sources is thus shown to be identical to a modal sum.

3.4. THE TOTAL AVERAGE INPUT IMPEDANCE FOR A TWO-DIMENSIONAL SYSTEM

The input impedances of the various mode groups have been established, and can be summed to give the input impedance of a two-dimensional cavity. This requires calculation of the terms in equation (3.21) for each mode separately, and the summation performed numerically for any enclosure of interest. In this section however, a closed form expression for the total average input impedance is derived. This requires knowledge of the λ_{M0} term for each mode group, i.e., the modal density for each group.

Consider the three different types of mode group: the $(0, 0)$ mode, the usual one-dimensional modes $(n, 0)$, $(0, m)$, and finally the majority of the modes (n, m), $n, m \neq 0$. An exact expression for the number of mode groups, M, in this last category cannot be derived in general terms, and has to be calculated numerically for each set of enclosure dimensions. However, an average rate at which new one-dimensional mode groups begin, $\mathrm{d}M/\mathrm{d}k$ can be calculated.

If in Figure 1, the radius is increased by δk, an area $\pi k \delta k/2$ is encompassed, leading to an increase in modes $\mathrm{d}N$, each of elemental area π^2/A, giving the usual modal density $\mathrm{d}N/\mathrm{d}k$ as

$$\mathrm{d}N/\mathrm{d}k = Ak/2\pi, \tag{3.22}$$

where N is the mode count at k for (n, m) modes. At wavenumber k the mode count N is composed of M different mode groups. $(\mathrm{d}M/\mathrm{d}k)\delta k$ new groups start in the interval δk. Each of these new groups has, by definition, a modal density of $1/k_{M0} = 1/k$. Therefore the rate of change of modal density $\mathrm{d}^2N/\mathrm{d}k^2$ must be the product of the increase of new groups and their modal density, or

$$\mathrm{d}^2N/\mathrm{d}k^2 = (1/k)\,\mathrm{d}M/\mathrm{d}k. \tag{3.23}$$

The rate of increase of new mode groups is given from equations (3.22) and (3.23) as

$$\mathrm{d}M/\mathrm{d}k = AK/2\pi. \tag{3.24}$$

This is the same rate as for the usual mode count in equation (3.22), which from a mode count perspective alone suggests no advantage in the grouping system. However, some differences are seen from the following impedance considerations. The average impedance of a single mode group of modal density k_M is given from equation (3.21), upon setting $\varepsilon_n \varepsilon_m = 4$, as

$$\bar{Z}_M(0) = Z_{00}(S_0/V)(2\pi/k_M). \tag{3.25}$$

The influence of a new group decreases with the starting wavenumber, k_M. The increase in average impedance $\delta\bar{Z}(0)$ from all new wave groups in a band is

$$\mathrm{Re}\{\delta\bar{Z}(0)\} = Z_{00}(S_0/V)(2\pi/k)(\mathrm{d}M/\mathrm{d}k)\delta k, \tag{3.26}$$

which, on substituting from equation (3.24) gives

$$\mathrm{Re}\{\mathrm{d}\bar{Z}(0)/\mathrm{d}k\} = Z_{00} S_0 A/V. \tag{3.27}$$

The real part of the mean point impedance is therefore

$$\mathrm{Re}\{\bar{Z}(0)\} = Z_{00}(S_0/V)(Ak + l_x + l_y). \tag{3.28}$$

The l_x and l_y terms are added as these refer to the $(n, 0)$ and $(0, m)$ groups. For non-dispersive waves, this equation tends to four times the value for a point source in an infinite two-dimensional space, for which the impedance is given [25] as

$$\text{Re}\,\{\bar{Z}(0)\} = \rho\omega S_0^2. \tag{3.29}$$

The factor of four occurs because of the four sources at the corner at the origin. The form of the impedance of equation (3.28) is shown in Figure 8. At zero wavenumber, there is no real impedance as the enclosure behaves as a spring (for rigid boundaries), and the higher order modes have not yet cut on. Equation (3.28) gives a non-zero value at zero frequency because it is an average value including the higher modes. When $k = k_b$, the $(n, 0)$ and $(0, m)$ mode groups begin causing a large step contribution, which is constant at all wavenumbers as indicated. Only two mode groups are required to describe these very important sets of modes. The transfer impedance in heavily damped media tend to be dominated by these 'least damped' modes, which have the shortest length across the cavity.

When $k = k_p$, the angled wave groups cut on. The increase in group start frequency is balanced by a decreasing contribution from each group causing the total impedance to increase with k. If no new groups were included in the summation beyond k_f, the impedance would start to drop below the true value, as indicated in the figure, but does not go to zero. The result is, however, accurate until $k = k_f$, unlike when a modal sum is used and many more modes are required at higher wavenumbers for accuracy.

4. MODIFIED TRANSFER FUNCTIONS

In equation (3.15) a transfer function was presented which corresponded to that used in the classical modal approach. Some reservations were noted on the grounds that the source lines used actually crossed the enclosure, giving an instantaneous response at remote positions with no time delay allowance. The problem is that for some conditions, a linear array of point sources spaced Δ_M apart cannot be regarded as a line source. This is a typical problem of arrays, but it is shown, for example in [20], that provided the perpendicular distance from the point source line is greater than the spacing, Δ_M, the wavefront is almost plane and so it appears to be generated by a line source. However, if the observer point is less than Δ_M from the sources the line source model is not valid, and the line source joining a particular linear array of point sources must be disregarded, because in the time domain the spherically spreading wavefront from a point source will not have reached the position of the equivalent line source. If there is light damping, most of the waves interfering to form modal patterns are derived from distant image sources whose influence is accurately represented by plane wave fronts, and so the modal representation and the one-dimensional approach developed are valid. However, when the damping becomes

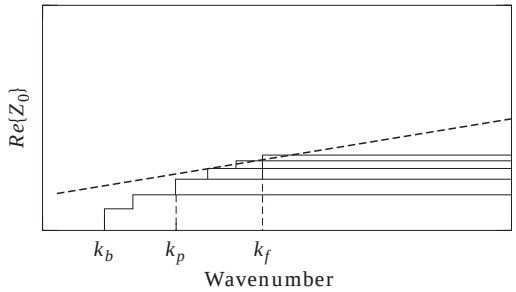

Figure 8. Real part of the point-impedance for a two-dimensional system.

heavy, the contribution from the true point source is larger than all other contributions and the enclosure behaves more like a free field. This case cannot be modelled with the method presented in section 3, but the purpose here is to present some justification for a modified model which will also accommodate the heavy damping case. To achieve this, the link between point sources and equivalent line sources must be established, and the reflection coefficients for wall absorption calculated.

4.1. LINE SOURCE REPRESENTATION

In reference [20] it was argued that the path length before wavefronts became plane was of the order of the source spacing Δ_M. Another similar definition is provided here, also using the time domain argument used in reference [20]. Consider an array of impulsive sources each giving energy E_0 over a small time duration Δ_T. The peak radiated velocity u at any point r, shown in Figure 9, is given by

$$E_0 = (p^2/\rho c)2\pi r\ \delta(t - r/c)\Delta_T \tag{4.1}$$

where the velocity u is related to the peak pressure by $p = \rho c u$.

Although arbitrary, one criterion for regarding the wavefront as plane is when the axial component of intensity at the intersection of wavefronts at point A in Figure 9 is the same as that normal to the source at point C. A second criterion is that A is sufficiently close to C for the wavefront to be approximately straight. The first criterion is met when

$$2u^2 \cos^2 \beta = u^2, \tag{4.2}$$

which gives an angle of $\beta = \pi/4$, and $r = \Delta_M / \sqrt{2}$. The pulse width in the time domain is spread to AC. The distance AC is $\sim 0{\cdot}3r$ which gives a wavefront approaching plane.

It is now possible to show how exclusion of all the line sources with exception of those with sufficiently small source spacings Δ_M can properly account for the close image source contribution to the sound field. The pressure from a line array with point sources can be calculated by noting that all the energy E_0 from a single source concentrates over a distance Δ_M in the plane wavefront at large distances; i.e.,

$$E_0 = (2p^2/\rho c)\Delta_T\ \delta(t - r/c)\Delta_M. \tag{4.3}$$

The factor of 2 allows for wavefronts in both directions spreading from the source line. The peak pressure from a single line source is given from equation (4.3) as

$$p = \sqrt{\rho c E_0 / 2\Delta_M}. \tag{4.4}$$

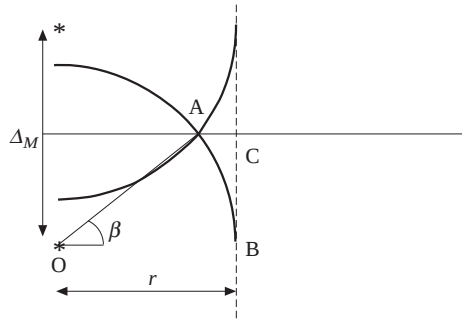

Figure 9. Wavefronts close to the image source lines. - - - - , Assumed wavefront.

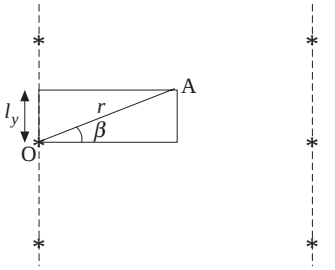

Figure 10. Line source representation of early image sources, *, Image sources; ----, line sources.

The peak pressure from a single point source at a distance r is given from equation (4.1) as

$$p = \sqrt{\rho c E_0 / 2\pi r}. \tag{4.5}$$

Consider an arbitrary rectangle of aspect ratio $\tan \beta$, shown in Figure 10. $\beta < \pi/4$, and the source spacing $\Delta_M = 2l_y$.

Only the line sources indicated contribute to the first arrival of a wave from the origin, O, to the far corner A. The pressure from the two line sources is given from equation (4.4) as

$$p_l = \sqrt{\rho c E_0 / r \sin \beta}. \tag{4.6}$$

The pressure from the four nearest image sources is given from equation (4.5) as

$$p_i = 1{\cdot}6\sqrt{pcE_0 / r}. \tag{4.7}$$

The ratio of the two results is shown in Figure 11, and lies between 1·35 and 0·8, giving equal responses when $\beta = \pi/7{\cdot}8$. The aspect angle β lies between the limits of a square enclosure ($\beta = \pi/4$) and one with an aspect ratio of approximately 5 ($\beta = \pi/16$). At larger aspect ratios (or smaller values of β), more point sources will contribute to the first arrival and so the comparison is inappropriate. This demonstrates that the complete contribution of the near sources can be attributed to the usual one-dimensional wave groups $(n, 0)$ and $(0, m)$. In the summation for the complete enclosure, all the line sources within a distance of $\Delta_M / \sqrt{2}$ are therefore not included. The $\Delta_M / \sqrt{2}$ criterion also allows estimates to be made for the limiting case of the square enclosure.

4.2. CALCULATION OF ANGLE DEPENDENT REFLECTION COEFFICIENTS

The general formulation, for example in equation (3.11), requires a single value $\bar{r}$ to describe the absorption by boundaries, of waves making a return journey over a distance λ_M. In practice this involves a combination of the mean reflection coefficients of four walls,

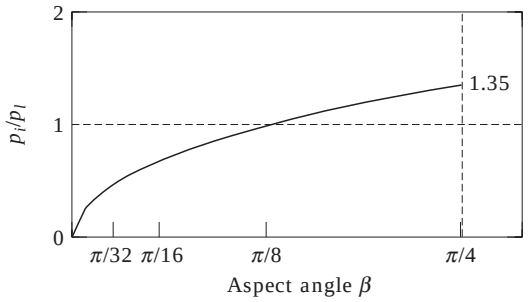

Figure 11. Ratio of line source and image source first arrival amplitude.

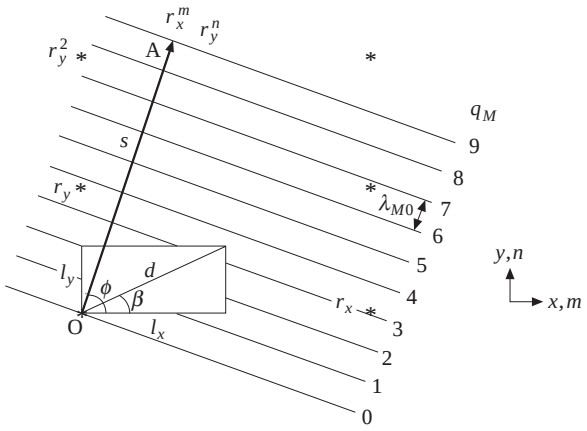

Figure 12. Image sources modified by reflection coefficient.

r_{1x}, r_{2x}, and r_{1y}, r_{2y} for wave components normal to the x and y directions, as shown in Figure 12. If a one-dimensional system as shown in Figure 6 has reflection coefficients r_1 and r_2 on the terminations at $x = 0$ and $x = 1$, then the equivalent reflection coefficient of one return journey is $\bar{r}_x = r_{1x}\, r_{2x}$. The four reflection coefficients for the four walls considered here can thus be reduced to two: r_x, r_y, as in Figure 12, for wave components in the x and y directions respectively.

The source counters in the x and y directions are m and n such that $2ml_x = x$, $2nl_y = y$. It is worth noting that the n, m integers are the same as those used in equation (2.2), only now they are associated with lengths rather than wavenumbers. m becomes the length counter in the x direction, and n the length counter in the y direction. The normalized source strength R at image (m, n) is therefore

$$R = r_x^m\, r_y^n. \tag{4.8}$$

The wavefront arriving at the origin from a line source passing through this point will have a source strength of the value given in equation (4.8). R will appear as a continuous function for distant sources because of the merging contribution

$$R = r_x^{x/2l_s}\, r_y^{y/2l_y} \tag{4.9}$$

from sources in a line. If the path distance to this line source from the origin is s, and the source line spacing is λ_{M0},

$$s = q\lambda_{M0}, \qquad q = 0, 1, 2, 3, \ldots, \tag{4.10}$$

the true source strength can be written with an angle dependence ϕ_p,

$$R = (\bar{r}_M)^q, \tag{4.11}$$

where $\bar{r}_M$ is the reflection coefficient for these parallel source lines for mode groups M,

$$\bar{r}_M = ((r_x)^{\cos\phi_p/\cos\beta}(r_y)^{\sin\phi_p/\sin\beta})^{\lambda_{M0}/2d} \tag{4.12}$$

where ϕ_p is given in equation (2.4). d seen in Figure 12 is the diagonal of the enclosure, which is at angle β. This is a slightly confusing result because it suggests that even for angle independent reflection coefficients r_x, r_y the modal reflection coefficient $\bar{r}_M$ is a function of both wave angle ϕ_p and the modal source line spacing. This would not occur in a one-dimensional system where the wave angle and source spacing are constant. However,

for two dimensions, changes in wave direction bring in a varying number of reflections from the x and y surfaces, thus altering the net contribution in equation (4.9).

If the wall reflection coefficients themselves are functions of the angle of incidence ϕ_p, i.e., $r_y = r_y(\phi_p)$ and $r_x = r_y(\pi/2 - \phi_p)$, then these values can be inserted directly into equation (4.12). Inspection of equation (4.12) would suggest that, as the source line spacing λ_{M0} decreases, i.e., for high order mode groups, the reflection coefficient would actually become closer to unity, giving less attenuation than for the lower order groups. If no account is taken of the distance travelled before a mode is established, as is suggested here, then it would appear that high order modes would be very significant, which is not the usual experience. However, because the wave group must travel a distance $s = \Delta_M/\sqrt{2}$ before becoming established as a mode in the enclosure, a factor of $\bar{r}_M^{q_M}$ is applied to all of the incoming waves, where q_M is the number of line sources in the interval $\Delta_M/\sqrt{2}$: i.e.,

$$q_M = (1/\sqrt{2})(\Delta_M/\lambda_{M0}) = Ak_M^2/\sqrt{2}\pi^2. \tag{4.13}$$

This actually gives very heavy attenuation for the high order waves before they are established as a mode. These relations, established from image source considerations, have not yet been confirmed by observation, as in the accompanying experimental work a rigid walled enclosure where $r_x = r_y = 1$ was used.

4.3. MODIFIED ONE-DIMENSIONAL MODEL

The one-dimensional model in Figure 6 can be modified to exclude all line sources that are closer than $\Delta_M/\sqrt{2}$ from the origin. The source integer q describes the nearest source line to be included, where $q = 0$ would correspond to a line source at the origin. The transfer impedance at any point x, excluding sources with integers less than q is obtained from a sum similar to that of equation (3.2).

$$Z_q(x) = \rho cS(\alpha^q + \alpha^{q+1} + \cdots)(e^{-ikx} + e^{ikx}), \quad q \geqslant 1, \tag{4.14}$$

or

$$Z_q(x) = \rho cS[2\alpha^q/(1-\alpha)]\cos kx. \tag{4.15}$$

If $q = 0$, the travelling wave from the origin is included:

$$Z_0(x) = Z_1(x) + \rho cS\, e^{-ikx}. \tag{4.16}$$

By following the same procedure in section 3, the pressure response at distance x_M from the source line at the origin in Figure 3 for the Mth wave group is found to be given from equations (4.15) and (3.15) as

$$p(x_M)/u_0 = (Z_{00}/\Delta_M t)[(2\alpha_M^{q_M}/(1-\alpha_M)]\cos kx_M, \tag{4.17}$$

where $\alpha_M = \bar{r}_M e^{-ik\lambda_{M0}}$, $\bar{r}_M$ is given in equation (4.12)

The nearest source line to be included is the integer q_M: $q_M \geqslant (1/\sqrt{2})(\Delta_M/\lambda_{M0})$. q_M is the lowest value possible by the criterion, which always excludes the first outgoing wave from the source. This outgoing wave can be described in two separate spatial zones as follows.

(i) If the observation point in the cavity at a distance r from the origin is $r < \Delta_{min}/\sqrt{2}$ where Δ_{min} is the minimum source spacing (e.g., $2l_y$ in Figure 10) then only the true source is contributing significantly and a point source term can be added to the mode group sum; the total response is then

$$\frac{p(r)}{u_0} = Z_{00}\sqrt{\frac{k}{2\pi r}}\, e^{-ikr} + Z_{00}\sum_M \frac{\varepsilon_n \varepsilon_m}{\Delta_M t}\frac{\alpha_M^{q_M}}{1-\alpha_M}\cos kx_M, \quad q_M \geqslant 1, \tag{4.18}$$

$\varepsilon_n \varepsilon_m = 2$ for the $(n, 0)$ and $(0, m)$ groups and $\varepsilon_n \varepsilon_m = 4$ for the (n, m) mode groups.

(ii) If the observation point in the cavity at a distance r from the origin is $r > \Delta_{min}/\sqrt{2}$, then the line source from the origin can contribute accurately as shown in section 4.1 and the total response includes the $q_M = 0$ term: i.e.,

$$\frac{p(r)}{u_0} = Z_{00} \frac{2}{\Delta_M t} e^{-ikx_M} + Z_{00} \sum_M \frac{\varepsilon_n \varepsilon_m}{\Delta_M t} \frac{\alpha_M^{q_M}}{1 - \alpha_M} \cos kx_M, \quad q_M \geqslant 1. \tag{4.19}$$

The two cases differ only in the first term, which will be significant only for very heavy damping, or for enclosures with large aspect ratios. The travelling wave term in equation (4.19) corresponds to the plane wave from the shortest length of the cavity. For a square cavity this must be multiplied by two, although the formulation would only be valid for the corner furthest from the origin.

The summation only has to include mode groups up to the upper wavenumber limit of k. For heavy damping only the free field term from the point source survives. For light damping, the modulus of α^{q_M} will be close to unity giving the usual modal behaviour, yet with a phase delay $e^{-ik\lambda_{M0}q_M}$ appropriate to each group of waves. This equation should be effective for both time and frequency representations of rectangular enclosures with either uniform wall absorption or medium absorption.

5. GENERAL APPLICATION

In the preceding theory only a very idealized example of a corner-excited, rectangular enclosure with absorbent boundaries has been considered. The intention was to obtain a physical understanding of the behaviour of this class of system, permitting a simplified analysis for non-ideal cases. However, a few observations can be made concerning the broader application of: a source not at the corner; three dimensions; and degenerate modes.

If the source is not located at the corner, the modal attenuation and path length are undisturbed. However, the fundamental equation (3.3) for the one-dimensional system will be slightly altered by an additional multiplicative interference term. For a rigid-walled enclosure this modifying factor would be expected to be $\cos k_x x_0 \cos k_y y_0$, where x_0, y_0 is the location of the source relative to the corner.

In principle, all the analyses carried out on a two-dimensional enclosure can be extended to model three-dimensional fields. A fully three-dimensional (oblique) mode in a three-dimensional rectangular enclosure comprises four pairs of opposing travelling waves. Each pair may be modelled as a one-dimensional system. Tangential (two-dimensional) modes may be modelled exactly as presented here, with the one-dimensional (axial) modes being treated accordingly.

Degenerate modes (distinct modes occurring at the same frequency) pose no significant problems for a non-square enclosure as they are handled separately in their respective groups. For a square enclosure, the modal density will be half that expected, so the impedance should be doubled.

6. EXPERIMENTS

Some experiments are reported here which were designed to conform to the unmodified theory, namely a moderately damped two-dimensional enclosure. An air-filled cavity was

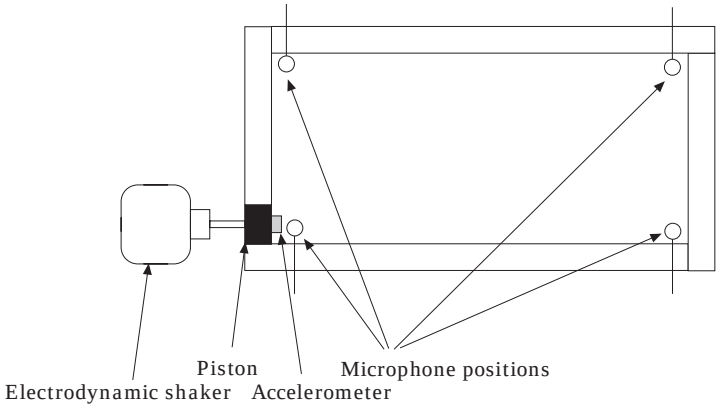

Figure 13. Two-dimensional perspex cavity.

used, with adjustable boundary positions and variable damping within the acoustic space. The cavity was made from two thick parallel perspex plates separated by a small gap across which the acoustic pressure was assumed to be constant. The boundaries were acoustically rigid. The cavity could be excited at one corner and the pressure measured at any point within.

6.1. EXPERIMENTAL PROCEDURE

The cavity used for all the experimental measurements is shown in Figures 13–15. It was made from two large 25 mm thick perspex sheets of area 1 m $\times$ 0·235 m separated by 25 mm square section perspex bars, giving a 25 mm air gap, which should mean that the cavity permits two-dimensional modes only until $\sim$6·8 kHz. It was thought that the thick perspex walls would provide a reflection coefficient close to unity. A gap was left in one corner to accommodate a small rectangular section perspex piston of face area 25 mm $\times$ 50 mm. The piston was instrumented with a light weight accelerometer on the inside surface. A small microphone could be positioned at any point inside the cavity.

With the microphone positioned close to the inner surface of the piston, the piston was excited with a stepped sine wave from 100 Hz to 3500 Hz (fully three-dimensional

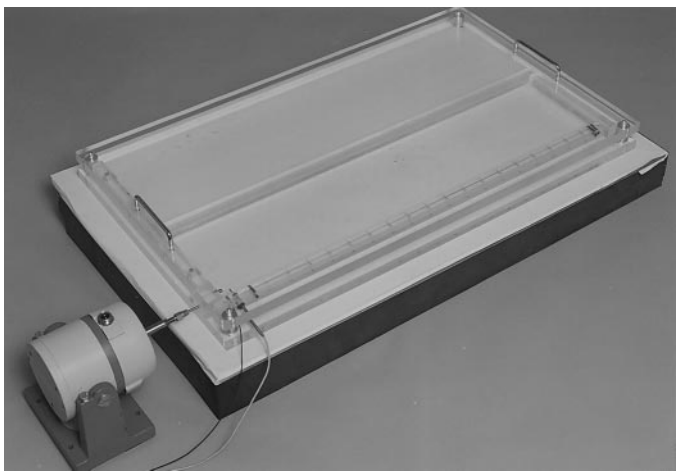

Figure 14. Two-dimensional perspex cavity; microphone in position for measurement of input impedance.

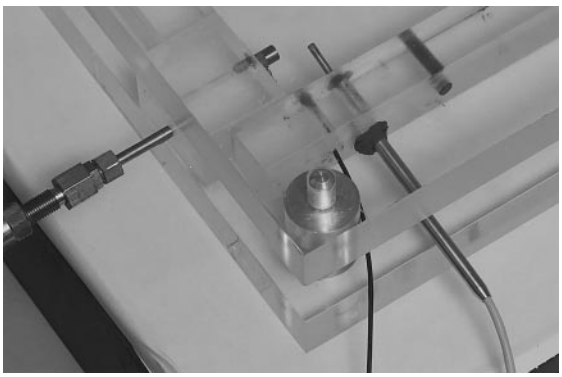

Figure 15. Two-dimensional perspex cavity; close-up of piston, accelerometer and microphone.

modes have not yet cut on at this upper frequency). The normalized measured input impedance was computed from the accelerometer and microphone data. This procedure was repeated with the microphone placed at each of three remaining corners of the cavity in turn, and the measured transfer impedance to those points was also calculated.

All the tests were repeated with the base of the cavity lined with (a) woodchip wallpaper; (b) 3 mm thickness felt. The effect of lining the cavity base was to introduce damping which was distributed evenly throughout the cavity area. This was done to simulate damping within the fluid itself.

6.2. RESULTS AND COMPARISON WITH THEORETICAL PREDICTIONS

The input impedance at one corner of the cavity was calculated, as was the transfer impedance to the remaining three corners. The modal damping for the three chosen conditions was also determined. Comparison between the experimental measurements and the theoretical predictions was made up to a frequency of 1500 Hz. Equations (3.11) and (3.15) were used to calculate the input and transfer impedances respectively, the result being doubled for two-dimensional mode groups. Identification of the modal frequencies and mode groups was carried out numerically using equation (2.2).

6.2.1. *Input impedance*

Plots of the real and imaginary parts of the measured normalized input impedance for zero added damping, medium added damping (paper base), and high added damping (felt base) are shown in Figures 16(a–c). For the zero and medium added damping, visual identification of the individual modes up to a frequency of approximately 1500 Hz was possible, and these have been labelled on the graphs. (n, m) refers to the number of half wavelengths in the length (x) and width (y) directions. Above this frequency the overlap of the modes becomes too high to render the identification accurate. For the high added damping, visual mode identification was only found to be possible for the first few modes and the first three are labelled.

The impedance for the first mode group between 0–700 Hz, given in equation (3.21), setting $\varepsilon_n \varepsilon_m = 2$, takes a theoretical mean value for $(n, 0)$ modes of

$$\bar{Z}_M = Z_{00} S_0 c/2Vf_{M0} \approx 36Z_{00}/f_{M0} \approx 0.1 \tag{6.1}$$

c is the speed of sound, V is the cavity volume, and f_{M0} is the frequency of the first resonance in the group (170 Hz in this case for the (1, 0) group), and Z_{00} is $\rho c S_0$. This average line

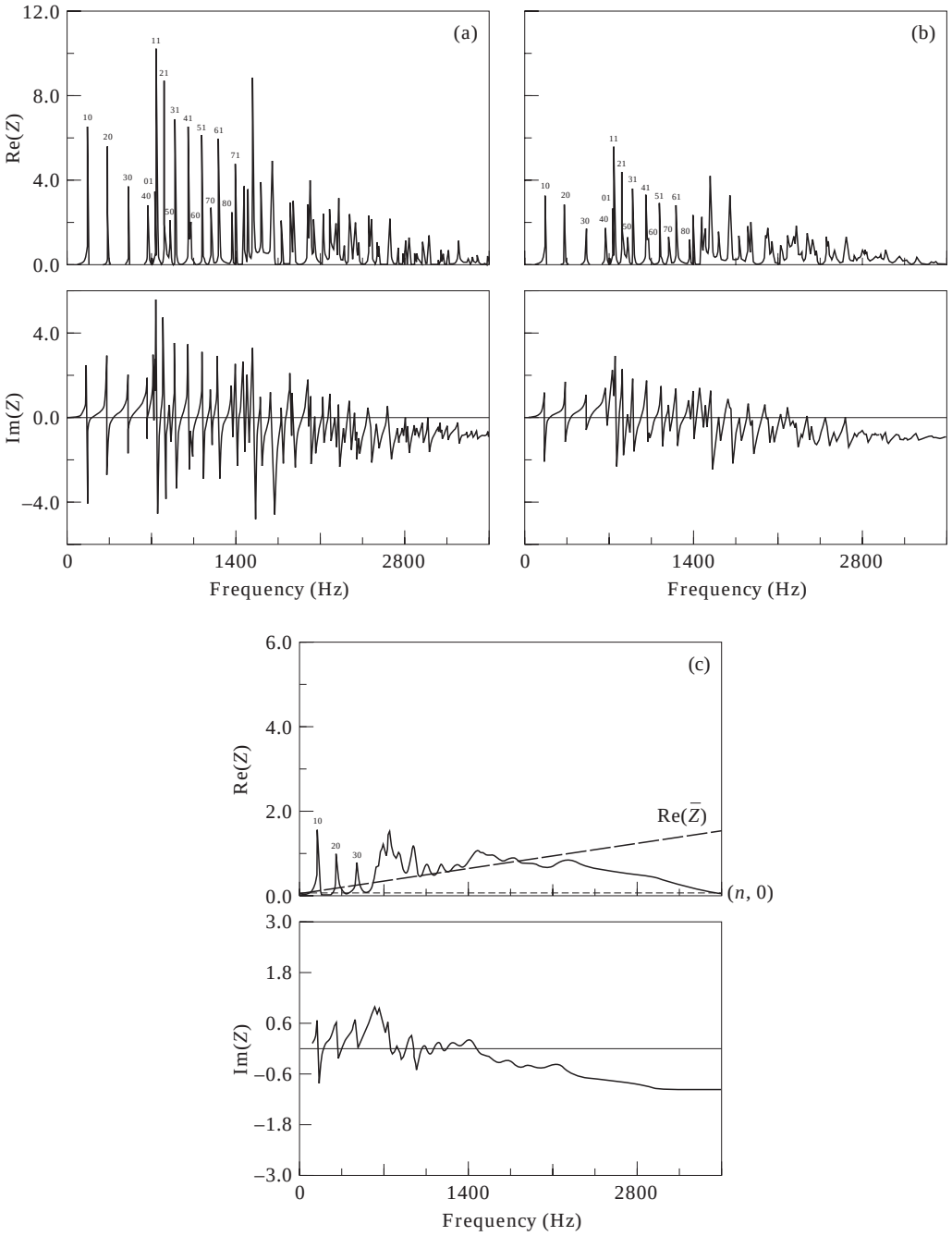

Figure 16. Normalized measured input impedance. (a) No added damping; (b) medium added damping (paper base); (c) high added damping (felt base).

is drawn in Figure 16(c) and its contribution can be seen relative to the total impedance over the whole frequency range. The next mode group to contribute is the $(0, m)$ group beginning at $f_{M0} = 723$ Hz. The frequency average value for these modes is given from equation (6.1) as $\sim 0{\cdot}025$. The first two-dimensional group (2, 1) begins close by at 743 Hz,

taking a mean value of approximately twice this, i.e., $\sim 0{\cdot}05$ ($\varepsilon_n \varepsilon_m = 4$). These groups, along with further $(n, 1)$ groups, control the response until 1457 Hz when the (1, 2) group begins.

Figure 16(c) also shows the expected value of the real part of the input impedance which is given in equation (3.28) as

$$\mathrm{Re}\,\{\bar{Z}(0)\} = Z_{00}\,(S_0/ct)2\pi f, \tag{6.2}$$

where t is the cavity depth.

This mean value is based on a high frequency assumption and is seen to be acceptable even at low frequencies. It can be seen, however, that above 1500 Hz the measured response ceases to climb as predicted. This is probably because the source has ceased to behave as a point source. A quarter wavelength will extend to the outer edge of the source piston, i.e., $\lambda = 4d$, where d is the piston diameter, at 1700 Hz. A quarter wavelength criterion has to be applied rather than a half wavelength as would be usual because the presence of the rigid boundary doubles the effective source length. At 3400 Hz a half wavelength extends across the piston giving the cancellation trends seen in Figures 16.

The imaginary parts of the impedance oscillate about the zero of each mode group but there is an increasing negative trend with increasing frequency. This is to be expected, as a pulsating cylinder in an infinite medium [25] has a stiffness controlled imaginary component of impedance, which is negative.

The damping can be seen to progressively increase in Figures 16(a), 16(b) and 16(c) as would be expected. The measured values of modal loss factor calculated from the half power points are shown in Table 1. For no added damping, the $(n, 0)$ modes seem to have a loss factor of approximately 0·01, which is about twice the mean value for the (n, m) modes. When the paper was added, the damping of the $(n, 0)$ modes increased to about 0·02. The (n, m) values increased by a similar amount to about 0·01. The felt produced such a large increase that only the $(n, 0)$ modes were measurable at a damping of about 0·065. The measured and predicted input impedances for each damping level are shown

TABLE 1

Measured modal loss factors

Modal frequency (Hz)	Mode numbers (n, m)	Loss factors		
		No damping	Medium damping	High damping
170	1, 0	0·0148	0·0260	0·0676
340	2, 0	0·0112	0·0196	0·0674
510	3, 0	0·0104	0·0196	0·0625
680	4, 0	0·0118	0·0181	—
723	0, 1	0·0060	—	—
743	1, 1	0·0064	0·0122	—
799	2, 1	0·0061	0·0122	—
850	5, 0	0·0134	0·0214	—
885	3, 1	0·0056	0·0108	—
993	4, 1	0·0057	0·0116	—
1020	6, 0	—	—	—
1116	5, 1	0·0051	0·0099	—
1190	7, 0	0·0065	0·0122	—
1250	6, 1	0·0049	0·0098	—
1360	8, 0	0·0047	0·0098	—
1392	7, 1	0·0044	0·0088	—

in Figure 17. As can be seen, the theoretical predictions show good agreement with the measured data at all three damping levels. The frequencies at which the modes occur and the peak levels have, in general, been reproduced.

In the predictions, a different modal loss factor was used for each mode group, the group modal loss factor chosen being equal to the average of the measured modal loss factors for that group where more than one modal loss factor was measured (for the (1, 0) group),

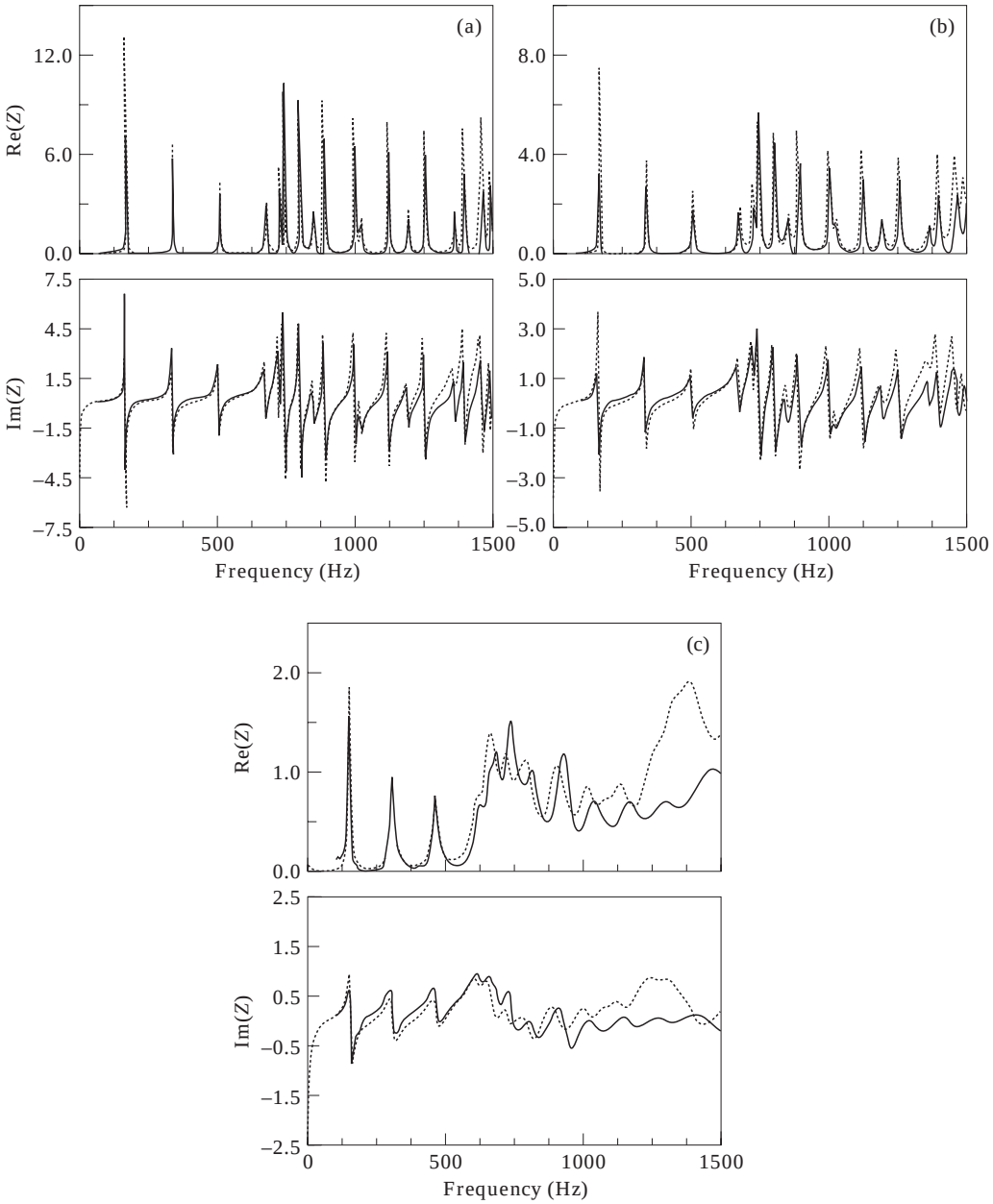

Figure 17. Normalized input impedance; comparison between measurements and predictions. (a) Zero added damping; (b) medium added damping (paper base): (c) high added damping (felt base). ——, Measurement, - - - - -, prediction.

and equal to the measured modal loss factor for groups where only one modal loss factor was measured. For the modes in the (1, 0) group, the measured modal loss factor tends to decrease with frequency. Therefore, for the lower modes in the group, the loss factor used in the predictions was too low, and for the higher modes within the group, it was too high. For all damping levels, this results in an overestimate of the peak heights for the lower modes in the group, and an underestimate of the peak heights for the higher modes in the group. This is evident in the graphs. However, even for the modes where the loss factor used in the predictions was equal to the measured loss factor (the (1, 1), (2, 1), (3, 1), (4, 1), (5, 1), (6, 1), and (7, 1) mode groups for zero and medium damping), in general, the predictions give an overestimate of the peak heights. This may be due to two causes.

(i) The boundary reflection coefficients in the measurement system are probably not unity, and this will lead to prediction errors. As can be seen from the graphs, these errors tend to decrease with the addition of damping. With added damping the fluid losses become large compared with the boundary losses (which remain unchanged on adding damping), so ignoring the boundary losses becomes less significant.

(ii) The discrepancies between the measurements and the predictions tend to increase with frequency. This may be caused because of the omission here of the real part of the attenuation term α_M^{qM} in equations (4.13) and (4.18). From Figures 17(a) and 17(b) it can be seen that, for similar frequencies, the peak heights for new mode groups cutting on ((1, 1), (2, 1), (3, 1), (4, 1), etc.) are more in error than the peak heights of modes belonging to older groups (modes (4, 0), (5, 0), (6, 0), (7, 0)). The effect of the attenuation term was calculated for new mode groups occurring at $\sim$1 kHz for loss factors 0·005, 0·01 and 0·065, corresponding to the average values for the (n, m) modes for the three cavity linings. For the untreated cavity the attenuation is $\sim$0·9; for the paper-lined cavity $\sim$0·8; and for the felt-lined cavity $\sim$0·3. For the light and medium damping cases, inclusion of these values would give slightly improved estimates. Inclusion of the corresponding term for the high damping case does not improve the estimates in the same manner. However, this may have been due to too high a loss factor (based on the first three modes only) being used for the (n, m) modes. Unfortunately, for all damping cases, insufficient tests were done to demonstrate this phenomenon conclusively.

For the high added damping, the measured modal frequencies were slighly lower than the predicted ones. The addition of the felt layer to the cavity base may not only have increased the potential for damping (manifested in an increase in modal loss factor), but it may also have introduced an added mass to the cavity due to coupling with the felt. This would effect a reduction in sound speed within the cavity which would lower the modal frequencies, which was not included in the theoretical model. The comparison shown in Figure 17((c) was therefore made between the measured data and a prediction which assumed a much lower sound speed, based on the modal frequencies of the first three measured modes. However, normalization is with respect to the original sound speed.

6.2.2. *Transfer impedance*

Plots of the real and imaginary parts of the transfer impedance to the corner $x = 0$, $y = 1_y$ are shown in Figures 18(a–c) for the zero, medium, and high added damping cases. In addition, the transfer impedances to the remaining two corners are shown in Figures 18(d) and 18(e) for the high damping case. The measurement and predictions are shown.

As for the input impedance, for all damping levels the modal frequencies have, in general been reproduced. The fact that the small errors tend to increase with frequency suggests that an appropriate value for the sound speed within the cavity was not used in the

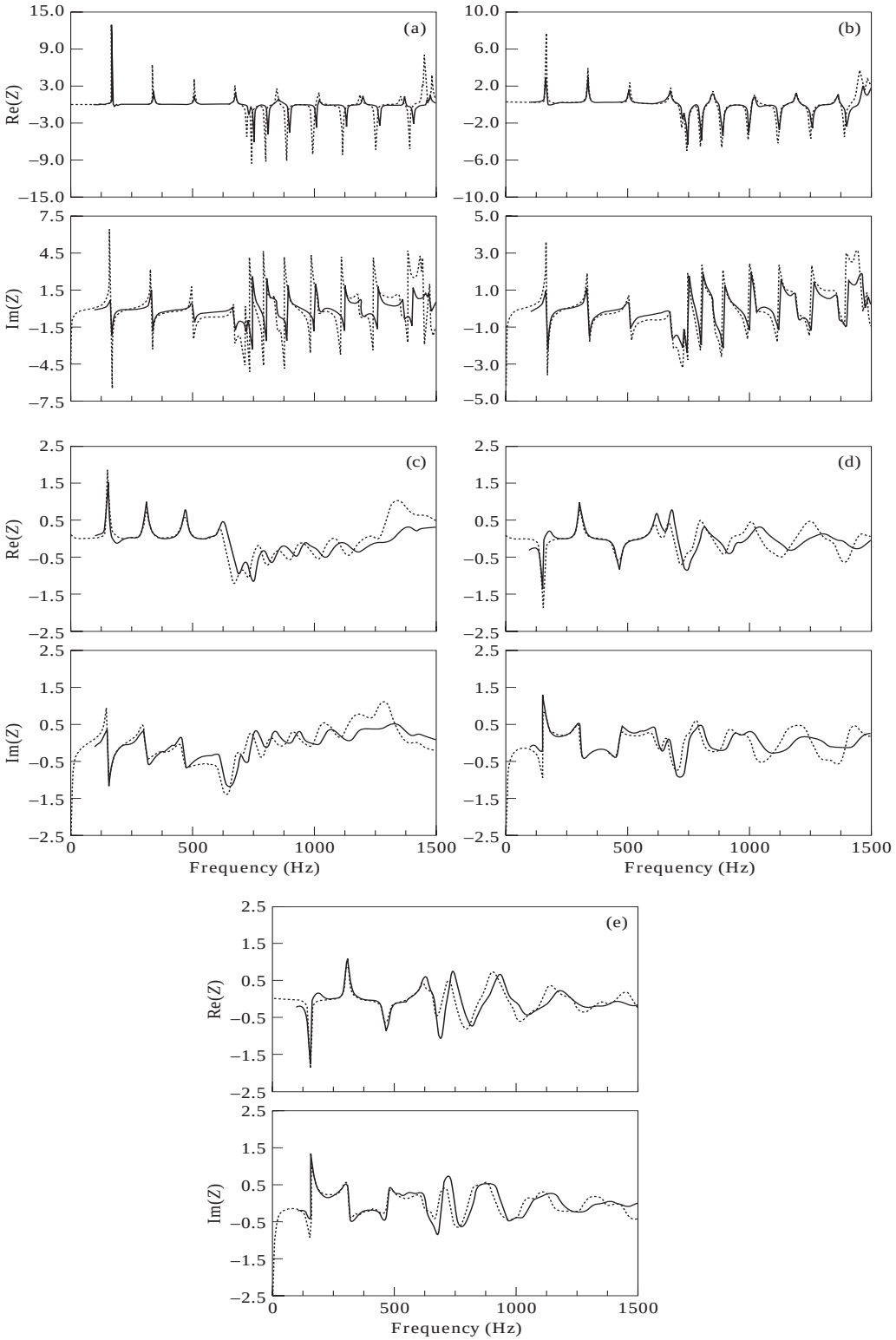

Figure 18. Normalized Transfer Impedance; comparison between measurements and predictions. (a) Zero added damping; (b) medium added damping (paper base); (c) high added damping (felt base); (d) high added damping (felt base); (e) high added damping (felt base). ——, Measurement; - - - - - , prediction. For (a), (b) and (c) transfer is to corner $x = 0$, $y = l_y$; for (d) transfer is to corner $x = l_x$, $y = l_y$; for (a) transfer is to corner $x = l_x$, $y = 0$.

predictions. This was unfortunately unavoidable due to the long duration of the experimental runs when the temperature (and hence sound speed) may have varied considerably.

For all transfer corners, at all damping levels, the signs of the peaks in both the real and imaginary parts of the transfer impedance have been reproduced correctly. This indicates that the phase terms in the impedance expressions derived earlier (equation (3.15)) are correct. However, the formulation which has been used does not reflect the time delay required for a line source to be set up. This is evident when the peak heights are investigated. The peak heights have not been reproduced exactly, and are in general lower in the measured data than in the predictions. As for the input impedance, this may be caused because of the omission here of the term α_M^{qM} in equation (4.18). As for the input impedance comparisons, the agreement between the measured data and the predictions improves for the higher damping cases. This again could be due to the fact that the boundaries do not have a unity reflection coefficient as was first assumed. With increased fluid damping, the relative importance of the boundary losses decreases, so the accuracy of the predictions improves.

7. CONCLUSIONS

This paper has investigated the basic nature of modes within a two-dimensional, damped vibratory system. An image source representation was used to model a corner-excited, rectangular system with either boundary or medium damping. Reduction of the point sources to arrays of line sources permitted the enclosure wave field to be modelled as a set of finite one-dimensional systems. Each one-dimensional system was shown to represent exactly a harmonic set of conventional modes. This demonstrated that the usual modal representation of a point source within a two-dimensional system assumes excitation by a lattice of line sources, and that furthermore, the image source model and the classical modal solution are related in a simple manner. Such a lattice excites the enclosure simultaneously giving acausal behavior. This problem is noticeable only with heavy damping when the wave field is dominated by the true point source, rather than the modes generated by distant image sources. The limitations of mode expansion with increased damping are thus clearly demonstrated and a physical interpretation provided.

The modal density of the equivalent one-dimensional systems and the point impedance were calculated and corresponded to expectation. Simple closed form expressions for the input impedance and corner transfer impedances were derived, thus demonstrating the power of the model in calculating transfer functions. This model has the advantage over the conventional modal model because it can more accurately represent damping and requires fewer terms for convergence. In addition, a possible way of dealing with angle dependent wall absorption is offered.

The acausal problem was resolved by excluding line sources which were closer than the spacing between two image sources on that line, on the basis that the wavefront from this set of sources would not be plane, and that a line representation would give a response before the arrival of the true wavefront. The outcome of the model is that mode groups that start at low wavenumbers suffer least attenuation and will dominate the transmission to other points, in the presence of damping in the medium or at the boundaries.

Finally, measurements were made on a rigid-walled, two-dimensional, rectangular, air filled cavity, excited at one corner, in order to validate the unmodified model. Both the input impedance and the transfer impedance to the corners of the cavity were investigated. The effect of damping, evenly distributed throughout the cavity, was also assessed. At all three damping levels investigated, the input and transfer impedance measurements showed

good agreement with theoretical predictions. Some estimates were made of the attenuation expected from the modified model, and although the outcome was of the correct order, there was insufficient data to demonstrate the attenuation phenomenon conclusively.

REFERENCES

1. J. R. Whiteman 1974 *The Mathematics of Finite Elements and Applications*. London: Academic Press.
2. M. Petyt, G. H. Koopman and R. J. Pinnington 1977 *Journal of Sound and Vibration* **53**, 71–82. The acoustic modes of a rectangular cavity containing a rigid, incomplete partition.
3. M. Petyt, J. Lea and G. H. Koopman 1976 *Journal of Sound and Vibration* **45**, 495–502. A finite element method for determining the acoustic modes of irregular shaped cavities.
4. A. Craggs 1972 *Journal of Sound and Vibration* **23**, 331–339. The use of simple three-dimensional acoustic finite elements for determining the natural modes and frequencies of complex shaped enclosures.
5. T. Shuku and K. Ishihara 1973 *Journal of Sound and Vibration* **29**, 67–76. The analysis of the acoustic field in irregularity shaped rooms by the finite element method.
6. M. Tohyama and S. Yoshikawa 1981 *Journal of the Acoustical Society of America* **70**, 1674–1678. Approximate formula of the averaged sound energy decay curve in a rectangular reverberant room.
7. H. Kuttruff 1973 *Room Acoustics*. London: Applied Science Publishers.
8. E. H. Dowell 1978 *Journal of the Acoustical Society of America* **64**, 181–191. Reverberation time, absorption and impedance.
9. A. Krokstad, S. Strøm and S. Sørsdal 1968 *Journal of Sound and Vibration* **8**, 118–125. Calculating the room response by the use of a ray tracing technique.
10. G. Benedetto and R. Spagnolo 1984 *Applied Acoustics* **17**, 365–378. Evaluation of sound absorbing coefficients in a reverberant room by computer-ray simulation.
11. A. M. Ondet and J. L. Barby 1989 *Journal of the Acoustical Society of America* **85**, 787–796 Modelling of sound propagation in fitted workshops using ray tracing.
12. J. J. Embrechts 1982 *Acustica* **51**, 288–295. Sound field distribution using randomly traced sound ray techniques.
13. M. Tajchert 1982 *Archives of Acoustics* **7**(3–4), 173–182. A geometrical-numerical method for the determination of the acoustic field properties related to the directions of reflected waves.
14. B. M. Gibbs and D. K. Jones 1972 *Acustica* **26**, 24–32. A simple image method for calculating the distribution of sound pressure levels within an enclosure.
15. M. Gensane and F. Santon 1979 *Journal of Sound and Vibration* **63**, 97–108. Prediction of sound fields in rooms of arbitrary shape: validity of the image sources method.
16. R. H. Lyon 1975 *Statistical Energy Analysis of dynamical systems*: *theory and applications*. MIT Press.
17. J. M. Muggleton and R. J. Pinnington 1990 *Journal of Sound and Vibration* **143**, 183–197. A low-frequency anechoic lining for underwater use.
18. J. M. Muggleton 1992 *Ph.D. Thesis*, *Southampton University*. Acoustic power flow in fluid filled tubes and cavities.
19. P. M. Morse 1936, 1948 *Vibration and Sound*. New York: McGraw-Hill.
20. C. G. Mayo 1952 *Acustica* **2**, 49–64. Standing wave patterns in studio acoustics.
21. F. J. Fahy 1985 *Sound and Structural Vibration*: *Radiation*, *Transmission and Response*. London: Academic Press.
22. C. L. Morfey 1986 in *Noise and Vibration* (edited by R. G. White and J. G. Walker). Theory of acoustics (II). Chichester: Ellis Horwood.
23. J. B. Allen and D. A. Berkley 1979 *Journal of the Acoustical Society of America* **65**, 943–950. Image method for efficiently simulating small-room acoustics.
24. I. S. Gradshteyn and I. M. Ryzhik 1980 *Tables of Integrals*, *Series and Products*. London: Academic Press.
25. S. N. Rschevkin 1963 *The Theory of Sound*. London: Pergamon Press.